Copyright © 1991, by the author(s).
All rights reserved.

Permission to make digital or hard copies of all or part of this work for personal or classroom use is granted without fee provided that copies are not made or distributed for profit or commercial advantage and that copies bear this notice and the full citation on the first page. To copy otherwise, to republish, to post on servers or to redistribute to lists, requires prior specific permission.

MODEL OF PLASMA IMMERSION ION IMPLANTATION FOR VOLTAGE PULSES WITH FINITE RISE- AND FALL-TIMES

by

R. A. Stewart and M. A. Lieberman

Memorandum No. UCB/ERL M91/14

21 February 1991
(Revised 12 June 1991)

MODEL OF PLASMA IMMERSION ION IMPLANTATION FOR VOLTAGE PULSES WITH FINITE RISE- AND FALL-TIMES

by

R. A. Stewart and M. A. Lieberman

Memorandum No. UCB/ERL M91/14

21 February 1991
(Revised 12 June 1991)

ELECTRONICS RESEARCH LABORATORY

College of Engineering
University of California, Berkeley
94720

MODEL OF PLASMA IMMERSION ION IMPLANTATION FOR VOLTAGE PULSES WITH FINITE RISE- AND FALL-TIMES

by

R. A. Stewart and M. A. Lieberman

Memorandum No. UCB/ERL M91/14

21 February 1991
(Revised 12 June 1991)

ELECTRONICS RESEARCH LABORATORY

College of Engineering
University of California, Berkeley
94720

ABSTRACT

In plasma immersion ion implantation, a target is immersed in a plasma and a series of negative, high-voltage pulses are applied to implant ions into the target. We develop an approximate analytical model to determine the time-varying implantation current, the total dose, and the energy distribution of the implanted ions for a voltage pulse with finite rise- and fall-times. Scaling rules are presented for the implanted current and energy distribution with respect to plasma density, peak applied voltage, and ion mass. Comparisons with numerical simulations are used to demonstrate that the accuracy of the model is well characterized by a single parameter: the ratio of the ion flight time to the pulse rise-time.

I. INTRODUCTION

Ion implantation has become a routine fabrication technique in semiconductor device manufacturing. In addition, metallurgical implantation is emerging as a technology in which new surface alloys are created to improve resistance to wear, corrosion and fatigue. Despite its widespread application, conventional ion implantation is not without drawbacks. Among these are ion source and beam scanning complexity and maintenance, low beam current, nonuniform implantation profile, and low energy efficiency per implanted ion.

In plasma immersion ion implantation (PIII), the intermediate stages of ion source, beam extraction, focusing, and scanning are omitted. The target is immersed in a plasma environment, and ions are extracted directly from the plasma and accelerated into the target by means of a series of negative, high-voltage pulses applied to the target. Both metallurgical[1-5] and semiconductor[6] implantation processes have been demonstrated using PIII.

Various analytical and numerical models of PIII have been developed[7-9] that determine the time-varying implantation current, the total dose, and the energy distribution of the implanted ions. For a rectangular voltage waveform applied to the target, an initial uniform density ion "matrix" sheath is assumed to form in the time scale of the inverse electron plasma frequency ω_{pe}^{-1}, as electrons are driven away. Subsequently, the sheath is assumed to grow in accordance with a quasistatic Child law[7].

In a realistic PIII experiment, the voltage pulse rise- and fall-times may constitute a significant fraction of the total pulse width ($\sim 0.5-3$ μs). In this case, the physical picture of a nearly instantaneous ion matrix sheath forming should be replaced by that of a gradually expanding, nonuniform sheath. The time evolution of this sheath determines the current $j(t)$ and the energy distribution dN/dW of implanted ions. Self-consistent equations have been solved numerically to find the time evolution of the sheath and the implanted current, as well as the energy distribution for non-abrupt voltage pulses in one-dimensional planar, cylindrical, and spherical geometries[8]. However, it is desirable to have an analytical estimate of j and dN/dW. In this study, we develop an approximate analytical model for a trapezoidal voltage pulse in one-dimensional planar geometry and compare the results with the numerical solutions. The model yields the time evolution of the sheath edge, the instantaneous implanted current, energy distribution, and total dose, plus their scalings with system parameters, that are useful in describing and implementing the PIII process. Additionally, the accuracy of the model is demonstrated to be characterized by a single parameter: the ratio of ion flight time to pulse rise-time.

II. BASIC MODEL

The applied voltage waveform is shown in Fig. 1 and is chosen to have the form

$$V(t)/V_o = \begin{cases} t/t_r \, , & 0 < t < t_r \\ 1 \, , & t_r < t < t_r + t_p \\ (t_t - t)/t_f \, , & t_r + t_p < t < t_t \end{cases} \quad . \tag{1}$$

where $t_t = t_r + t_p + t_f$. The pulse is characterized by three different times: rise-time t_r, plateau-time t_p, and fall-time t_f. Initially, the planar target is immersed in a uniform plasma of density n_o. For $t > 0$ (Fig. 2), the applied voltage causes plasma electrons to be pushed away from the electrode, resulting in the formation of an expanding, nonuniform sheath. The model assumptions are as follows:

(1) The ion flow is collisionless. This is valid for sufficiently low pressures.

(2) The electron motion is inertialess. This follows because the characteristic implantation time scale much exceeds ω_{pe}^{-1}.

(3) The applied voltage $V \le V_o$ is much greater than the electron temperature T_e during nearly the entire pulse duration; hence the Debye length $\lambda_D \ll s$ (except for $t \gtrsim 0$) and the sheath edge at s is abrupt.

(4) A quasistatic Child law sheath forms instantaneously at $t = 0^+$ and exists during the entire implantation. The current demanded by this sheath is supplied entirely by the uncovering of ions at the moving sheath edge[9].

(5) During the flight of an ion across the sheath, the electric field $E(x)$ is frozen at its value at the beginning of the flight.

Assumptions (3) (for $t \gtrsim 0$), (4) and (5) are approximations that permit an analytical solution to the sheath problem. The conditions for which these assumptions are justified will be presented in Section VI by comparison with numerical results.

III. SHEATH MOTION

The Child law current density j_c for a voltage V across a sheath of thickness s is[10,11]

$$j_c = \frac{4}{9}\epsilon_o\left(\frac{2e}{M}\right)^{1/2}\frac{V^{3/2}}{s^2} , \tag{2}$$

where ϵ_o is the free-space permittivity and e and M are the ion charge and mass. Equating j_c to the charge per unit time crossing the sheath boundary,

$$en_o\frac{ds}{dt} = j_c , \tag{3}$$

the sheath velocity is

$$\frac{ds}{dt} = \frac{2}{9}\frac{s_o^2 u_o}{s^2(t)}\tilde{V}^{3/2}(t) , \tag{4}$$

where

$$s_o = (2\epsilon_o V_o/en_o)^{1/2} \tag{5}$$

is the characteristic sheath thickness,

$$u_o = (2eV_o/M)^{1/2} \tag{6}$$

is the characteristic sheath (and ion) speed, and

$$\tilde{V}(t) = V(t)/V_o \tag{7}$$

is the normalized voltage waveform.

To proceed, (4) must be integrated to obtain the sheath motion $s(t)$. For convenience in the remaining analysis, we introduce a normalized time $T = \omega_{pi} t$. Integrating (4), with $s(0) = 0$, $\widetilde{V}(t) = t/t_r$ from (1), and using the relation

$$\omega_{pi} = u_o/s_o \;, \tag{8}$$

we obtain

$$S(T) = \left(\frac{4}{15}\right)^{1/3} T^{5/6}/\,T_r^{1/2} \;, \qquad 0 < T < T_r \;. \tag{9}$$

where $S = s/s_o$ is the normalized sheath thickness. Equation (9) is a relation for the sheath motion during the rise-time of the pulse, $0 < T < T_r$. During the pulse plateau, $T_r < T < T_r + T_p$, $s(t)$ is found by integrating (4) from T_r to T with $\widetilde{V}(t) = 1$ to obtain

$$S^3(T) = S^3(T_r) + \tfrac{2}{3}(T - T_r) \;. \tag{10}$$

Solving for $S(T_r)$ from (9) and inserting into (10) yields,

$$S(T) = \left[\frac{2}{3}\left(T - \frac{3}{5}T_r\right)\right]^{1/3}, \qquad T_r < T < T_r + T_p \;. \tag{11}$$

Finally, during the pulse fall-time, $T_r + T_p < T < T_t$, integrating (4) from $T_r + T_p$ to T, with $\widetilde{V}(t) = (t_t - t)/t_f$ yields

$$S(T) = \left[\frac{2}{3}T_p + \frac{4}{15}(T_r + T_f) - \frac{4}{15}(T_t - T)^{5/2}/\,T_f^{3/2}\right]^{1/3},$$

$$T_r + T_p < T < T_t \quad (12)$$

where $S(T_r + T_p)$, found from (11), was used. Equations (9), (11) and (12) provide a complete description of the sheath edge position for the duration of the applied voltage pulse. Note from (4) that since $\widetilde{V}(t)$ and the $s(t)$ given by (9), (11) and (12) are continuous functions of time, ds/dt given by (4) is also continuous, hence $s(t)$ is a smoothly varying function with continuous first derivative.

IV. QUASISTATIC IMPLANTATION

To calculate the current, following the approach in reference 7, we consider implanted ions having initial normalized positions $X_o = x_o/s_o$, reached by the expanding sheath edge at time $T_s = \omega_{pi}t_s$. Setting $S(T) = X_o$ at $T = T_s$, we find

$$X_o = S(T_s) \quad (13)$$

or, inverting

$$T_s = f(X_o)\ , \quad (14)$$

where $f(X_o)$ represents symbolically the inverse of (9), (11) or (12).

At time T_s, an ion begins its flight across the sheath. The ion flight time with the sheath assumed frozen at $T = T_s$ is given by[11]

$$T' = \frac{3X_o}{\widetilde{V}^{1/2}(T_s)}\ . \quad (15)$$

Hence, an ion at X_o reaches the target at a time T given by $T = T_s + T'$ or

$$T = g(X_o) \tag{16}$$

where

$$g(X_o) = f(X_o) + \frac{3X_o}{\tilde{V}^{1/2}(T_s)} . \tag{17}$$

Taking d/dX_o of (16), we obtain the implantation current density $j = en_o \, dx_o/dt$ as

$$j(t) = en_o u_o \left[\frac{dg(X_o)}{dX_o}\right]^{-1} . \tag{18}$$

The normalized current density $J(T) = j(t)/en_o u_o$ is found by solving (16) for X_o and inserting the result into (18).

From (16) and (18) it can be seen that continuity of $J(T)$ requires continuity both of $g(X_o)$ and $dg(X_o)/dX_o$. It can be shown that the second requirement leads to the further requirement of continuity of $d\tilde{V}(T)/dT$. Hence, we use the following smoothed approximation to $\tilde{V}(T)$ from (1) in (17):

$$V(t)/V_o \approx \begin{cases} \dfrac{t/t_r}{\left[1 + (t/t_r)^8\right]^{1/8}} , & 0 < t < t_r + t_p/2 \\[2ex] \dfrac{(t_t - t)/t_f}{\left\{1 + [(t_t - t)/t_f]^8\right\}^{1/8}} , & t_r + t_p/2 < t < t_t \end{cases} \tag{19}$$

We now apply the preceding procedure to obtain analytical expressions for the implanted current density. Since the sheath is assumed frozen during the ion flight, we use t_s as our reference time both for choosing the appropriate sheath model (9), (11) or (12), and for choosing the appropriate voltage function from (19).

(1) $T_s < T_r$

Letting $S = X_o$ and $T = T_s$ in (9) yields

$$T_s = \left(\frac{15}{4}\right)^{2/5} X_o^{6/5}\, T_r^{3/5} \; . \tag{20}$$

T' is found by letting $T = T_s$ in the first expression in (19) and inserting the resulting function $\widetilde{V}(T_s)$ into (15) to obtain

$$T' = 3\,X_o\left(\frac{T_s}{T_r}\right)^{1/2}\left[1 + (T_s/T_r)^8\right]^{1/16}. \tag{21}$$

Thus, $g(X_o) = T = T_s + T'$ becomes

$$T = g(X_o) = T_s + 3\,X_o\left(\frac{T_s}{T_r}\right)^{1/2}\left[1 + (T_s/T_r)^8\right]^{1/16}. \tag{22}$$

where $T_s(X_o)$ is given by (20). Taking d/dX_o of (20) we obtain

$$\frac{dT_s}{dX_o} = \frac{6}{5}\,T_s/X_o \; . \tag{23}$$

Taking d/dX_o of (22) and using (23) to evaluate (18), we find the normalized current density

$$J(T) = \left\{\frac{6}{5}\,T_s/X_o + \frac{6}{5}\left(\frac{T_s}{T_r}\right)^{-1/2}\left[1 + (T_s/T_r)^8\right]^{1/16} \right.$$
$$\left. + \frac{9}{5}\left(\frac{T_s}{T_r}\right)^{15/2}\left[1 + (T_s/T_r)^8\right]^{-15/16}\right\}^{-1} . \tag{24}$$

As described previously, $J(T)$ is found by solving (20) and (22) for the root X_o as a

function of T, and then inserting the result into (20) and (24).

(2) $T_r < T_s < T_r + T_p/2$

Here we use (11) for $S(T)$ but $\widetilde{V}(T_s)$ is unchanged from case (1) above. Letting $S = X_o$ and $T = T_s$ in (11) yields

$$T_s = \frac{3}{5}T_r + \frac{3}{2}X_o^3 \; . \tag{25}$$

Since $\widetilde{V}(T_s)$ is unchanged from case (1), (22) is still valid, but T_s is now given by (25). We again take d/dX_o of (22), but now using (25) we find

$$\frac{dT_s}{dX_o} = \frac{9}{2}X_o^2 \; , \tag{26}$$

and thus $J(T)$ becomes

$$J(T) = \left\{\frac{9}{2}X_o^2 + 3\left(\frac{T_s}{T_r}\right)^{-1/2}\left[1 + (T_s/T_r)^8\right]^{1/16} - \frac{27}{4}\frac{1}{T_r}X_o^3\left(\frac{T_s}{T_r}\right)^{-3/2}\left[1 + (T_s/T_r)^8\right]^{1/16} + \frac{27}{4}\frac{1}{T_r}X_o^3\left(\frac{T_s}{T_r}\right)^{13/2}\left[1 + (T_s/T_r)^8\right]^{-15/16}\right\}^{-1} . \tag{27}$$

(3) $T_r + T_p/2 < T_s < T_r + T_p$

For this interval, $S(T)$ is still given by (11), hence (25) is still the correct expression for T_s. However, $\widetilde{V}(T_s)$ is now obtained from the second expression in (19), which when inserted in (15) leads to

$$g(X_o) = T_s + 3X_o\left(\frac{T_t - T_s}{T_f}\right)^{-1/2}\left[1 + \left(\frac{T_t - T_s}{T_f}\right)^8\right]^{1/16}. \tag{28}$$

Taking d/dX_o of (28) and using (26), we find

$$\begin{aligned} J(T) = \Bigg\{ & \frac{9}{2}X_o^2 + 3\left(\frac{T_t - T_s}{T_f}\right)^{-1/2}\left[1 + \left(\frac{T_t - T_s}{T_f}\right)^8\right]^{1/16} \\ & + \frac{27}{4}\frac{1}{T_f}X_o^3\left(\frac{T_t - T_s}{T_f}\right)^{-3/2}\left[1 + \left(\frac{T_t - T_s}{T_f}\right)^8\right]^{1/16} \\ & - \frac{27}{4}\frac{1}{T_f}X_o^3\left(\frac{T_t - T_s}{T_f}\right)^{13/2}\left[1 + \left(\frac{T_t - T_s}{T_f}\right)^8\right]^{-15/16}\Bigg\}^{-1}. \end{aligned} \tag{29}$$

(4) $T_r + T_p < T_s < T_t$

For this case, we use (12) for $S(T)$. Letting $S = X_o$ and $T = T_s$ in (12) yields

$$T_s = T_t - T_f^{3/5}\left[\frac{5}{2}T_p + T_r + T_f - \frac{15}{4}X_o^3\right]^{2/5}. \tag{30}$$

$\widetilde{V}(T_s)$ is unchanged from case (3), hence (28) is still applicable, but with T_s given by (30). We again take d/dX_o of (28), but now using (30) we find

$$\frac{dT_s}{dX_o} = \frac{9}{2}X_o^2\left(\frac{T_t - T_s}{T_f}\right)^{-3/2}, \tag{31}$$

and thus $J(T)$ becomes

$$\begin{aligned} J(T) = \Bigg\{ & \frac{9}{2}X_o^2\left(\frac{T_t - T_s}{T_f}\right)^{-3/2} + 3\left(\frac{T_t - T_s}{T_f}\right)^{-1/2}\left[1 + \left(\frac{T_t - T_s}{T_f}\right)^8\right]^{1/16} \\ & + \frac{27}{4}\frac{1}{T_f}X_o^3\left(\frac{T_t - T_s}{T_f}\right)^{-3}\left[1 + \left(\frac{T_t - T_s}{T_f}\right)^8\right]^{1/16} \end{aligned}$$

$$- \frac{27}{4}\frac{1}{T_f} X_o^3 \left(\frac{T_t - T_s}{T_f} \right)^5 \left[1 + \left(\frac{T_t - T_s}{T_f} \right)^8 \right]^{-15/16} \Bigg\}^{-1} . \tag{32}$$

V. ENERGY DISTRIBUTION

From assumption (5), ions starting at position X_o at time T_s are implanted with energy

$$W = V(T_s) , \tag{33}$$

where W is in units of volts and here the exact voltage waveform (1) is used.

(1) $T_s < T_r$

From (1) and (33), ions entering the sheath at T_s are implanted with energy

$$W = V_o(T_s/T_r) . \tag{34}$$

Inverting, we find

$$T_s = T_r(W/V_o) . \tag{35}$$

Inserting (35) into (20) and solving for W yields

$$W = V_o \left(\frac{15}{4} \right)^{2/5} X_o^{6/5} T_r^{-2/5} . \tag{36}$$

Within the energy interval

$$dW = \frac{6}{5}\left(\frac{15}{4}\right)^{2/5} V_o X_o^{1/5} T_r^{-2/5} dX_o \ , \tag{37}$$

there are $dN = n_o dx_o$ ions per unit area implanted. Hence, we find

$$\frac{dN}{dW} = \frac{5}{6}\left(\frac{4}{15}\right)^{2/5} \frac{n_o s_o}{V_o} X_o^{-1/5} T_r^{2/5} \ . \tag{38}$$

Using (36) in (38), we find the energy distribution for ions entering the sheath during the pulse rise-time:

$$\frac{dN}{dW} = \left(\frac{25}{162}\right)^{1/3} \frac{n_o s_o T_r^{1/3}}{W^{1/6} V_o^{5/6}} \ . \tag{39}$$

(2) $T_r < T_s < T_r + T_p$

Ions entering the sheath during the voltage plateau receive the full energy V_o, hence

$$\frac{dN}{dW} = n_o s_o (S_p - S_r)\,\delta(W - V_o) \tag{40}$$

where

$$S_r \equiv S(T_r) = \left(\frac{4}{15}\right)^{1/3} T_r^{1/3} \tag{41}$$

is the normalized sheath position at the end of the rise-time and

$$S_p \equiv S(T_r + T_p) = \left[\frac{2}{3} T_p + \frac{4}{15} T_r\right]^{1/3} \tag{42}$$

is the normalized sheath position at the end of the plateau-time.

(3) $T_r + T_p < T_s < T_t$

From (1) and (33), ions entering the sheath at T_s are implanted with energy

$$W = V_o(T_t - T_s)/T_f \,. \tag{43}$$

Inverting, we find

$$T_s = T_t - T_f(W/V_o) \,. \tag{44}$$

Inserting (44) into (30) and solving for W yields

$$W = V_o\left[1 + T_r/T_f + (5/2)\,T_p/T_f - (15/4)\,X_o^3/T_f\right]^{2/5} . \tag{45}$$

Taking the differential of (45) and using $dN = n_o dx_o$, we find

$$\frac{dN}{dW} = -\frac{2}{9} n_o s_o \frac{T_f W^{3/2}}{V_o^{5/2}} \left[\frac{2}{3} T_p + \frac{4}{15}(T_r + T_f) - \frac{4}{15} T_f (W/V_o)^{5/2}\right]^{-2/3} . \tag{46}$$

A quantity of much interest in PIII is $f(W_{min})$, the fraction of ions that hit the target with $W < W_{min} < V_o$. Integrating (39) and (46) from 0 to W_{min}, we obtain

$$f = \left(\frac{4}{15}\right)^{1/3} T_r^{1/3}(W_{min}/V_o)^{5/6}/S_t + 1$$

$$- \left[1 - \frac{4}{15} T_f \left(W_{min} / V_o \right)^{5/2} / S_t^3 \right]^{1/3}, \tag{47}$$

where $S_t = S(T_t)$ is the normalized position of the sheath at the end of the fall-time and we have normalized f by the total dose $n_o s_o S_t$.

VI. DISCUSSION

(1) Scaling

Using a voltage waveform such as in Fig. 1 somewhat limits our ability to state precisely how the current density scales with plasma density and ion mass. Nevertheless, a set of restricted scaling rules can be given. For a fixed $J(T)$, the current density,

$$j(t) = e n_o u_o J(T) \tag{48}$$

scales as $n_o u_o$, or using (6),

$$j \propto n_o V_o^{1/2} M^{-1/2}. \tag{49}$$

From Section IV [see equations (25) and (27), for example], $J(T)$ remains fixed only when T_r, T_p, and T_f are fixed. Hence, we require that

$$T_x = \omega_{pi} t_x \propto n_o^{1/2} M^{-1/2} t_x \tag{50}$$

remain fixed, where $x = r$, p and f, in order for the scaling of (49) to remain valid. Thus, for a particular ion species, the plasma density and total pulse width must be simultaneously adjusted, while keeping the ratios t_r/t_p and t_f/t_p unchanged.

If we characterize the energy distribution by the fraction f, defined by (47) and considered a function of the normalized energy W_{min}/V_o, then the energy distribution is invariant with respect to changes in plasma density and ion mass, and is only a function of the ratios t_r/t_p and t_f/t_p. This can be seen from (47) by noting that both S_t and $T^{1/3}$ scale linearly with ω_{pi}.

(2) Comparison with Numerical Results

A PC-based numerical code has recently been developed[8] that solves the PIII implantation problem for non-abrupt voltage pulses of the form in (1). The nonlinear partial differential equations for the ion and electron motion are solved with the following simplifying assumptions: the ions are cold and their motion is collisionless, the electrons are in thermal equalibrium, and Poisson's equation relates the densities to the potential. The equations are

$$\frac{\partial n_i}{\partial t} + \frac{\partial}{\partial x}(n_i u_i) = 0 ,$$

$$M\left(\frac{\partial u_i}{\partial t} + u_i\frac{\partial u_i}{\partial x}\right) = -e\frac{\partial \Phi}{\partial x} ,$$

$$n_e = n_o \exp(-\Phi/T_e) ,$$

$$\frac{\partial^2 \Phi}{\partial x^2} = -\frac{e}{\epsilon_o}(n_i - n_e) .$$

Figures 3-5 show comparisons between the numerical results and the model for a wide range of ion masses and plasma densities. The voltage waveform in each case is given by V_o = 30 kV, t_r = 0.2 μs, t_p = 0.8 μs, and t_f = 0.3 μs. Note that the agreement between the analytical model and the numerical solution is best in Figs. 3(a)-(b) and

poorest in Figs. 5(a)-(b). Figures 3-5 have been grouped according to a particular value of the parameter β, defined by

$$\beta \equiv t'/t_r, \tag{51}$$

where t' is the ion flight time corresponding to the instant $j(t) = j_{max}$. The parameter β characterizes the severity of the approximation implicit in model assumption (5). For a given rise-time t_r, β (or t') scales as

$$\beta \propto s_o/u_o = \omega_{pi}^{-1} \tag{52}$$

or

$$\beta \propto M^{1/2} n_o^{-1/2}. \tag{53}$$

Returning to Figs. 3-5, which are plotted for $\beta = 0.1, 0.5, 1.0$, respectively, we note that both (a) and (b) for a given figure yield nearly identical fits between model and numerical result, despite having greatly different ion masses and plasma densities. Hence, the accuracy of the instantaneous implanted current density obtained from the analytical model is well characterized by the smallness of β (which in practice ranges from $\sim$ 0.1-1.0). We note also that model assumption (4) becomes valid more quickly during an implant for smaller β.

A qualitative explanation for the discrepancies between model and numerical results in Figs. 3-5 can be given by examining the implications of assumption (5) more closely. During the pulse rise-time, the model underestimates the electric field $E(x,t)$ felt by an ion during its flight, hence the model underestimates the ion current collected on the electrode during the interval $0 < t < t_r + t'$. Note that $E(x,t)$ is an increasing function of t since from (1), the voltage increases as $V(t) \sim t$ during the rise-time, while

from (9), the sheath edge expands only as $s(t) \sim t^{5/6}$. During the pulse fall-time, the model overestimates the electric field felt by an ion during its flight, hence the model overestimates the collected ion current for $t \gtrsim t_r + t'$. In contrast, during most of the pulse plateau, the model agrees very well with the numerical results for all values of β.

As a final comment regarding the current density, we note that the predicted scaling of $j \propto V_o^{1/2}$ is verified numerically.

In Fig. 6, the energy distributions obtained from both the model and numerical calculation are compared. The fraction f of ions implanted with $W < W_{min} < V_o$ is plotted versus t_r/t_p for voltage waveforms with $t_r = t_f$, $t_r + t_p = 1.0$ μs, and $V_o = 30$ kV, in an argon plasma with $n_o = 10^{10}$ cm^{-3}. Overall, the agreement is quite good. For this example, the model somewhat underestimates the fraction of implanted ions with energies $W < W_{min} \approx 0.6\,V_o$ since all ions entering the sheath during the pulse plateau are assumed to receive the full energy V_o. This error is seen to decrease as t_r/t_p increases, corresponding to smaller β values. Hence, β characterizes the agreement between the model and numerical results for the energy distribution. From Fig. 6 we also see that the model overestimates the fraction of very low energy ions, consistent with assumption (5) for $t \gtrsim 0$, and the dominance of the first term in (47) noted earlier.

ACKNOWLEDGEMENTS

This work was supported by a gift from Applied Materials, Inc. and a grant from the California Office of Competitive Technology. We are grateful to G. A. Emmert for the use of his numerical code. Helpful discussions with A. H. Sato are also gratefully acknowledged.

REFERENCES

[1]J. R. Conrad and C. Forest, in *IEEE International Conference on Plasma Science,* Saskatoon, Canada, May 19-21, 1986 (IEEE, New York).

[2]J. R. Conrad and T. Castagna, Bull. Am. Phys. Soc. **31**, 1479 (1986).

[3]J. R. Conrad, J. L. Radtke, R. A. Dodd, F. J. Worzala, and N. C. Tran, J. Appl. Phys. **62**, 4591 (1987).

[4]J. R. Conrad, S. Baumann, R. Fleming, and G. P. Meeker, J. Appl. Phys. **65**, 1707 (1989).

[5]J. Tendys, I. J. Donnelly, M. J. Kenny, and J. T. A. Pollack, Appl. Phys. Lett. **53**, 2143 (1988).

[6]X. Y. Qian, N. W. Cheung and M. A. Lieberman, To be published in *The Proceedings of the VIII International Conference on Ion Implantation Technology,* University of Surrey, United Kingdom, July 31-August 3, 1990.

[7]M. A. Lieberman, J. Appl. Phys. **66**, 2926 (1989).

[8]G. A. Emmert, in *IEEE International Conference on Plasma Science,* Oakland, CA, May 21-23, 1990 (IEEE, New York).

[9]J. T. Scheuer, M. Shamim, and J. R. Conrad, J. Appl. Phys. **67**, 1241 (1990).

[10]C. D. Child, Phys. Rev. **32**, 492 (1911).

[11]C. K. Birdsall and W. B. Bridges, *Electron Dynamics of Diode Regions* (Academic, New York, 1966).

[12]From equations (10) and (13) one can show that the sheath speed ds/dt is much greater during the pulse rise-time than during the fall-time. Hence, many more ions enter the sheath (and are subsequently implanted) during the rise-time than during the fall-time.

FIGURE CAPTIONS

Figure 1. Applied voltage waveform [—— equation (1); — equation (19)].

Figure 2. Planar PIII geometry showing the ion density n in a growing quasistatic Child law sheath.

Figure 3. Current density versus time for β = 0.1, V_o = 30 kV, t_r = 0.2 μs, t_p = 0.8 μs, t_f = 0.3 μs, and (a) n_o = 10^{10} cm^{-3}, M = 1 amu; (b) n_o = 5.5x10^{11} cm^{-3}, M = 40 amu (— numerical solution; --- analytical solution).

Figure 4. Current density versus time for β = 0.5, V_o = 30 kV, t_r = 0.2 μs, t_p = 0.8 μs, t_f = 0.3 μs, and (a) n_o = 1.7x10^{10} cm^{-3}, M = 40 amu; (b) n_o = 10^{10} cm^{-3}, M = 24 amu (— numerical solution; --- analytical solution).

Figure 5. Current density versus time for β = 1.0, V_o = 30 kV, t_r = 0.2 μs, t_p = 0.8 μs, t_f = 0.3 μs, and (a) n_o = 2.8x10^{9} cm^{-3}, M = 40 amu; (b) n_o = 10^{10} cm^{-3}, M = 160 amu (— numerical solution; --- analytical solution).

Figure 6. Fraction f of ions hitting the target with energies $W < W_{min}$ versus t_r/t_p, with W_{min}/V_o as a parameter, for the example of $t_r = t_f$, $t_r + t_p$ = 1.0 μs, V_o = 30 kV, n_o = 10^{10} cm^{-3}, and M = 40 amu (• numerical solution; --- analytical solution).

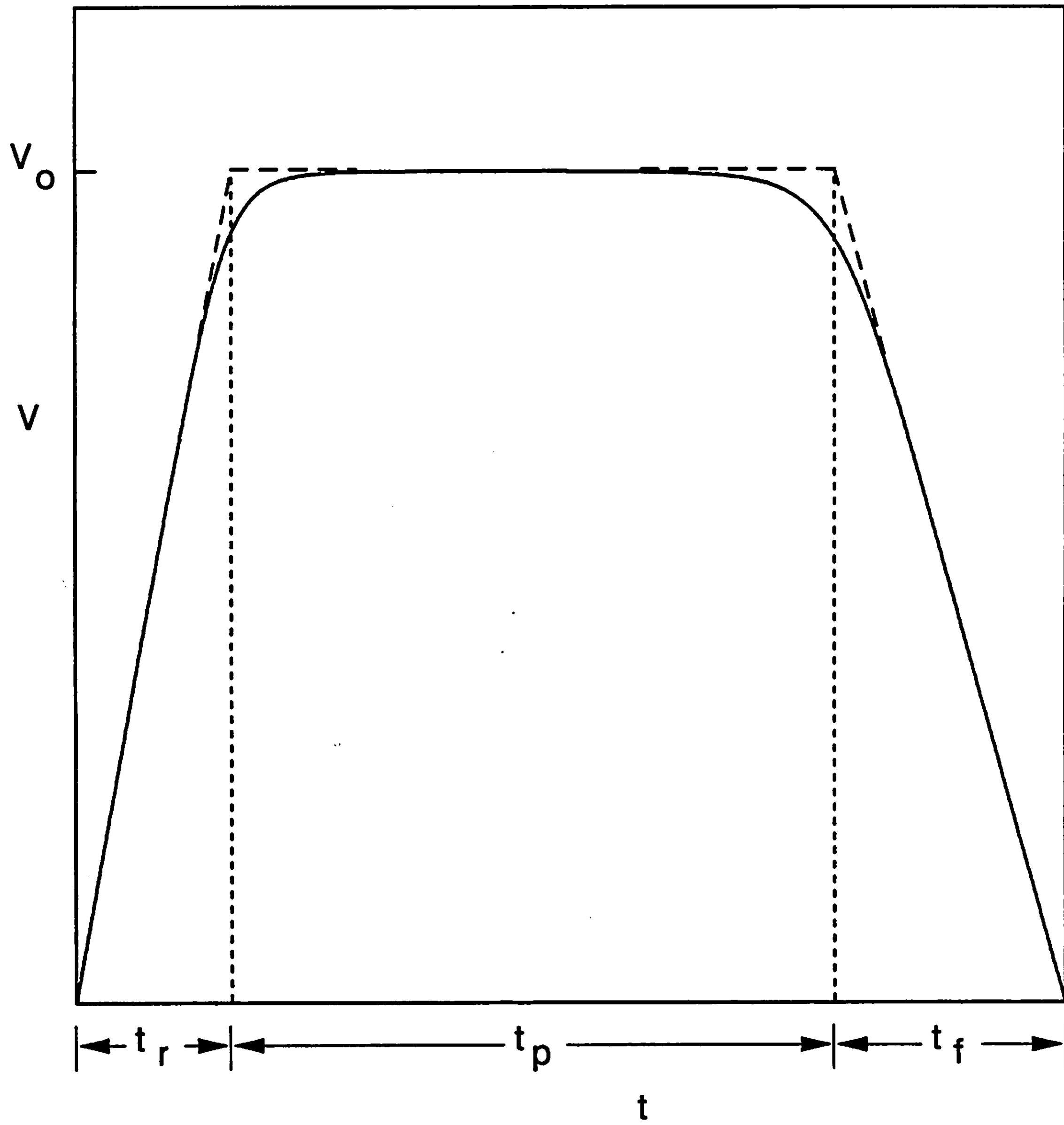

Figure 1

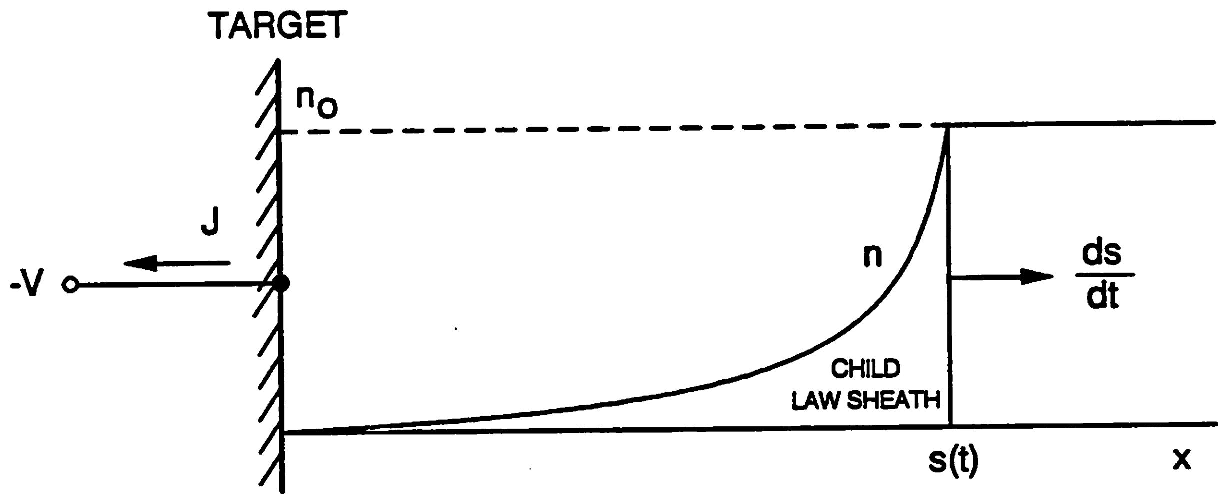

Figure 2

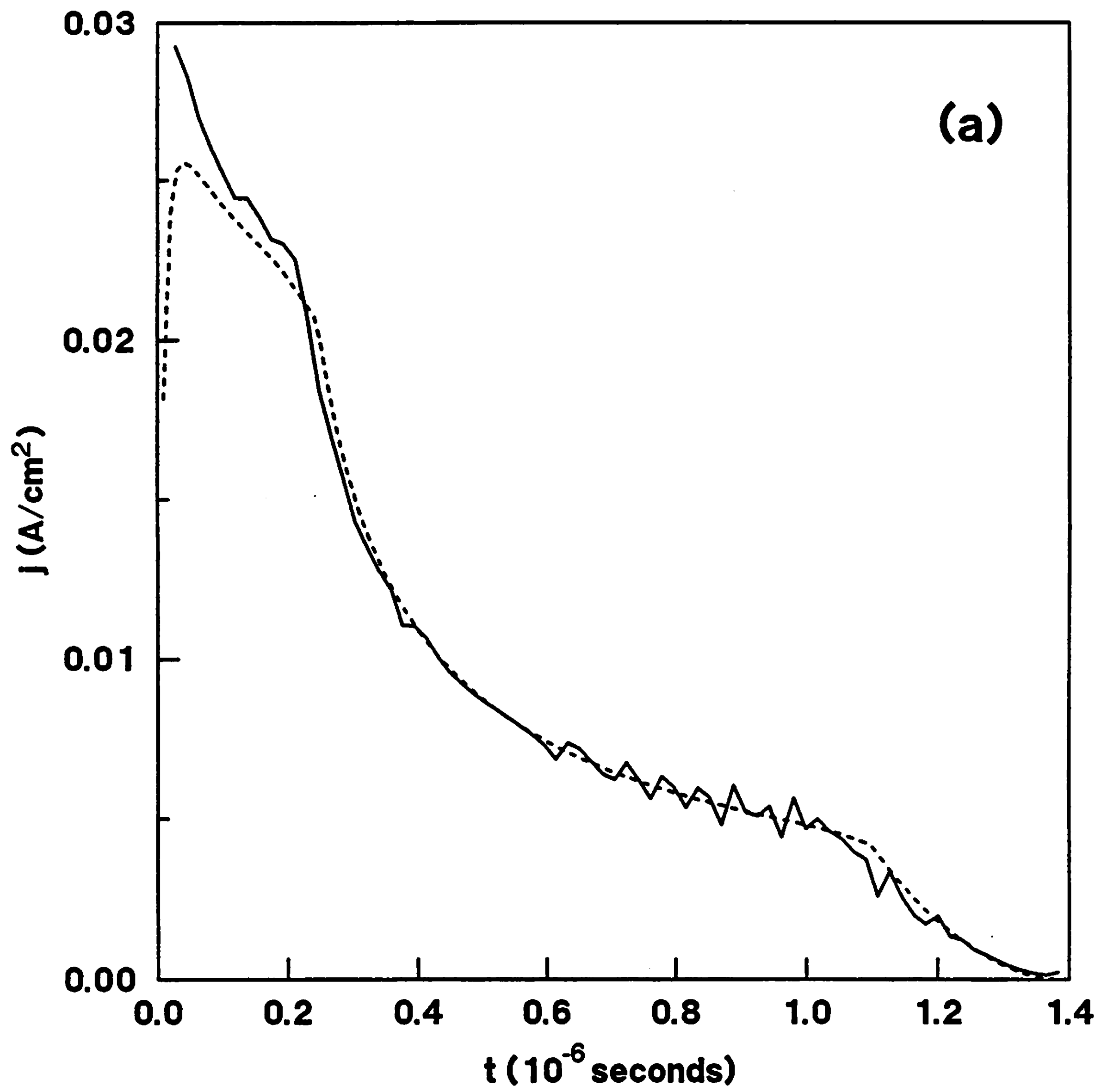

Figure 3(a)

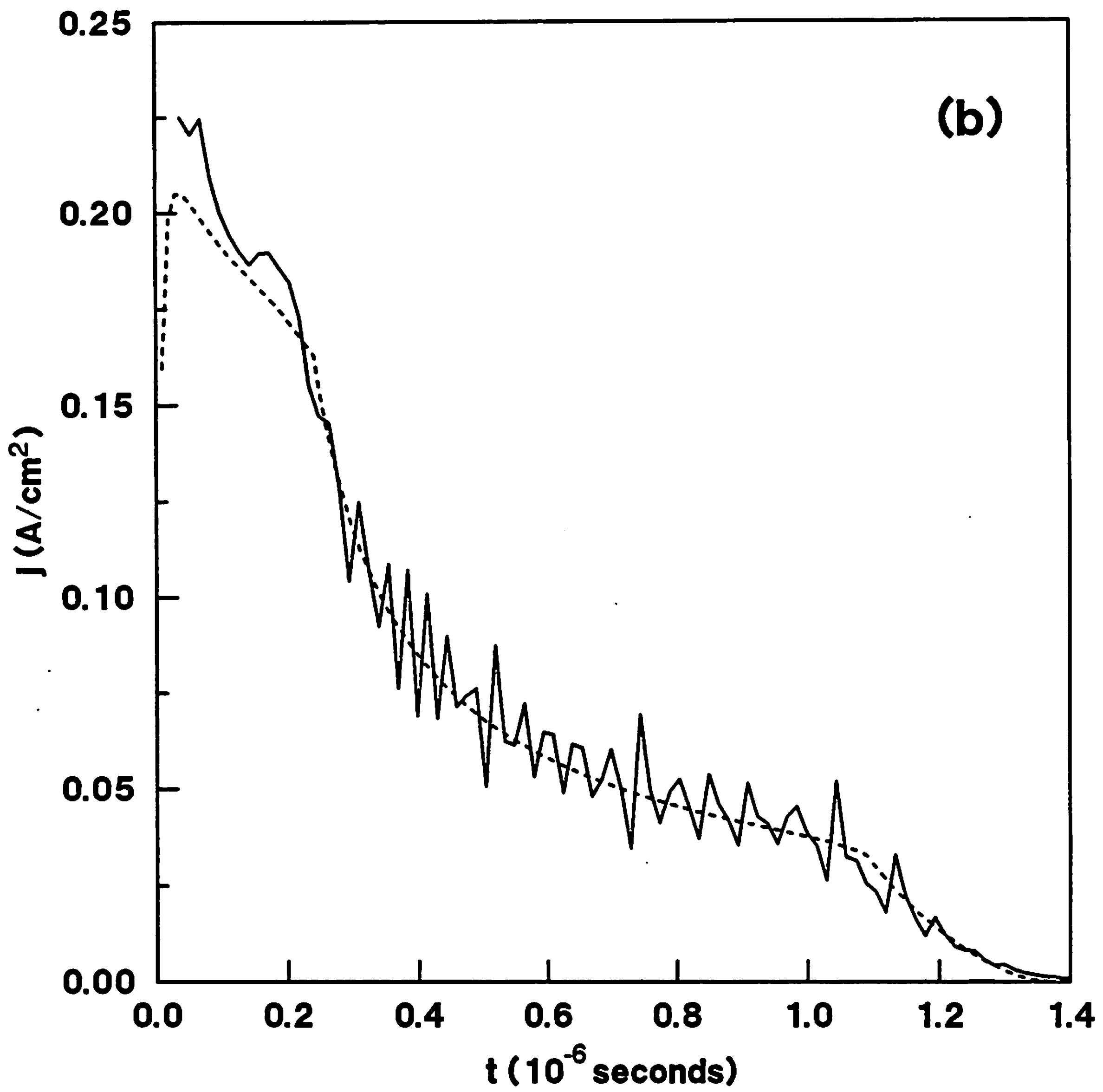

Figure 3(b)

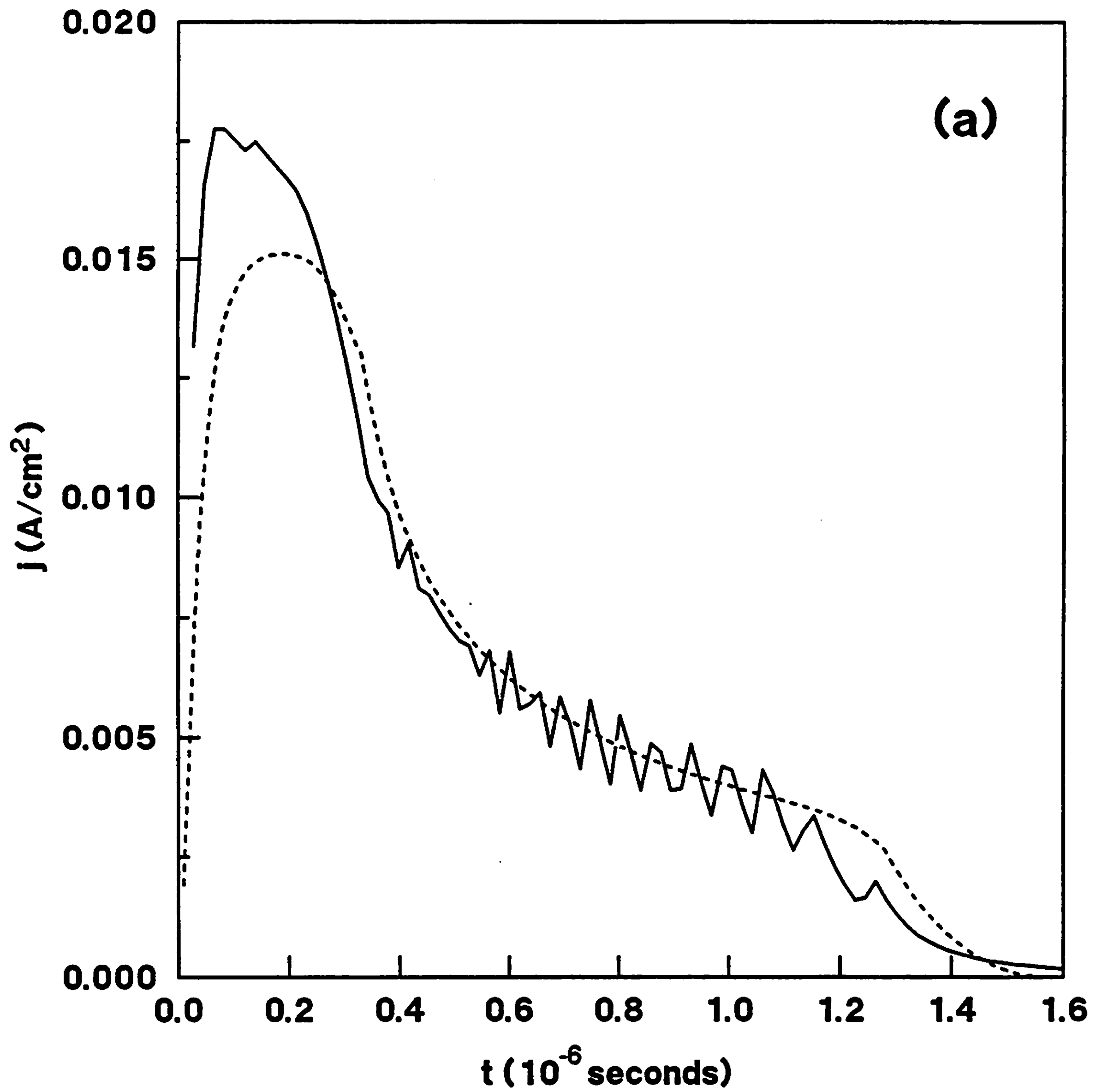

Figure 4(a)

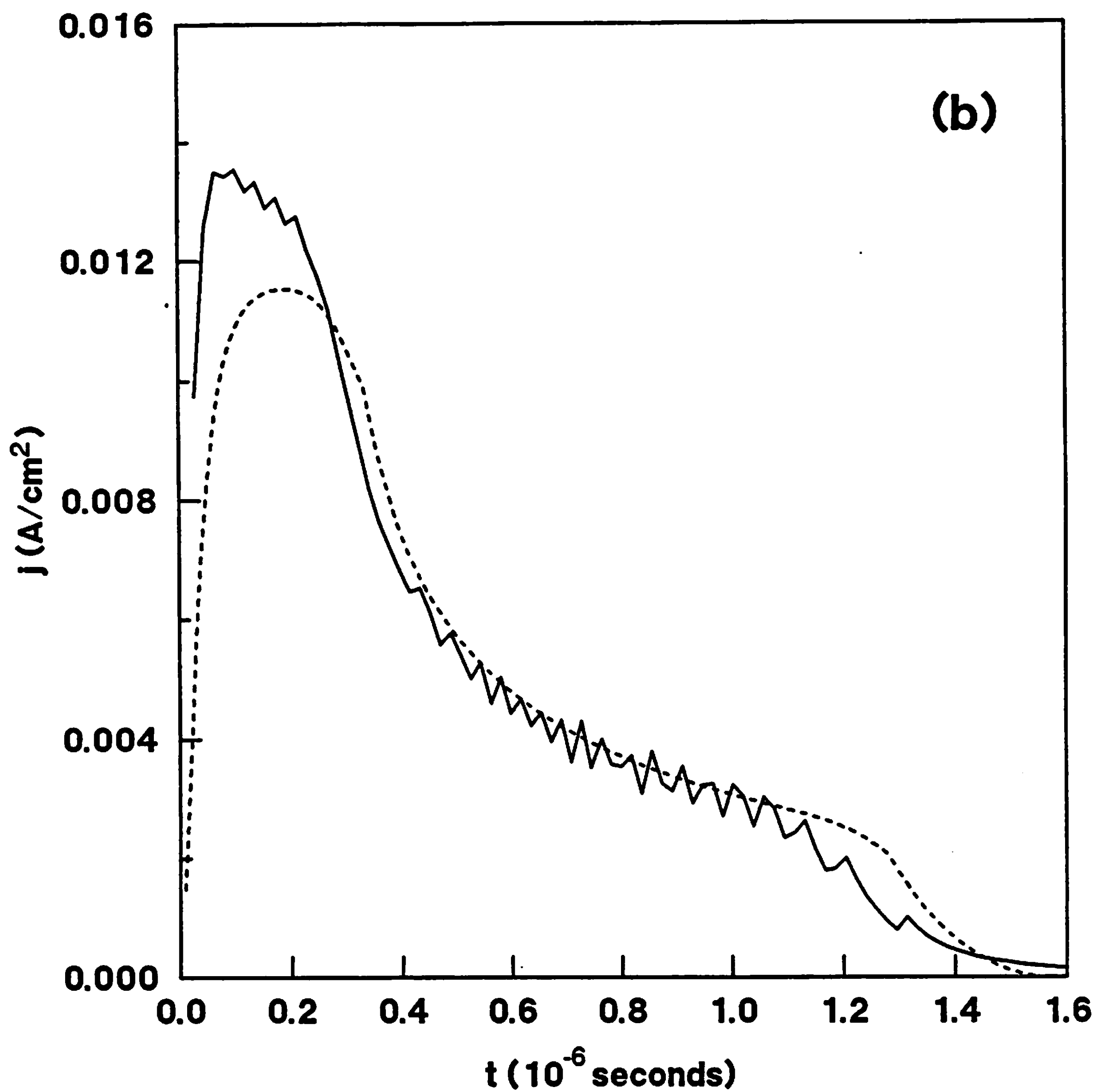

Figure 4(b)

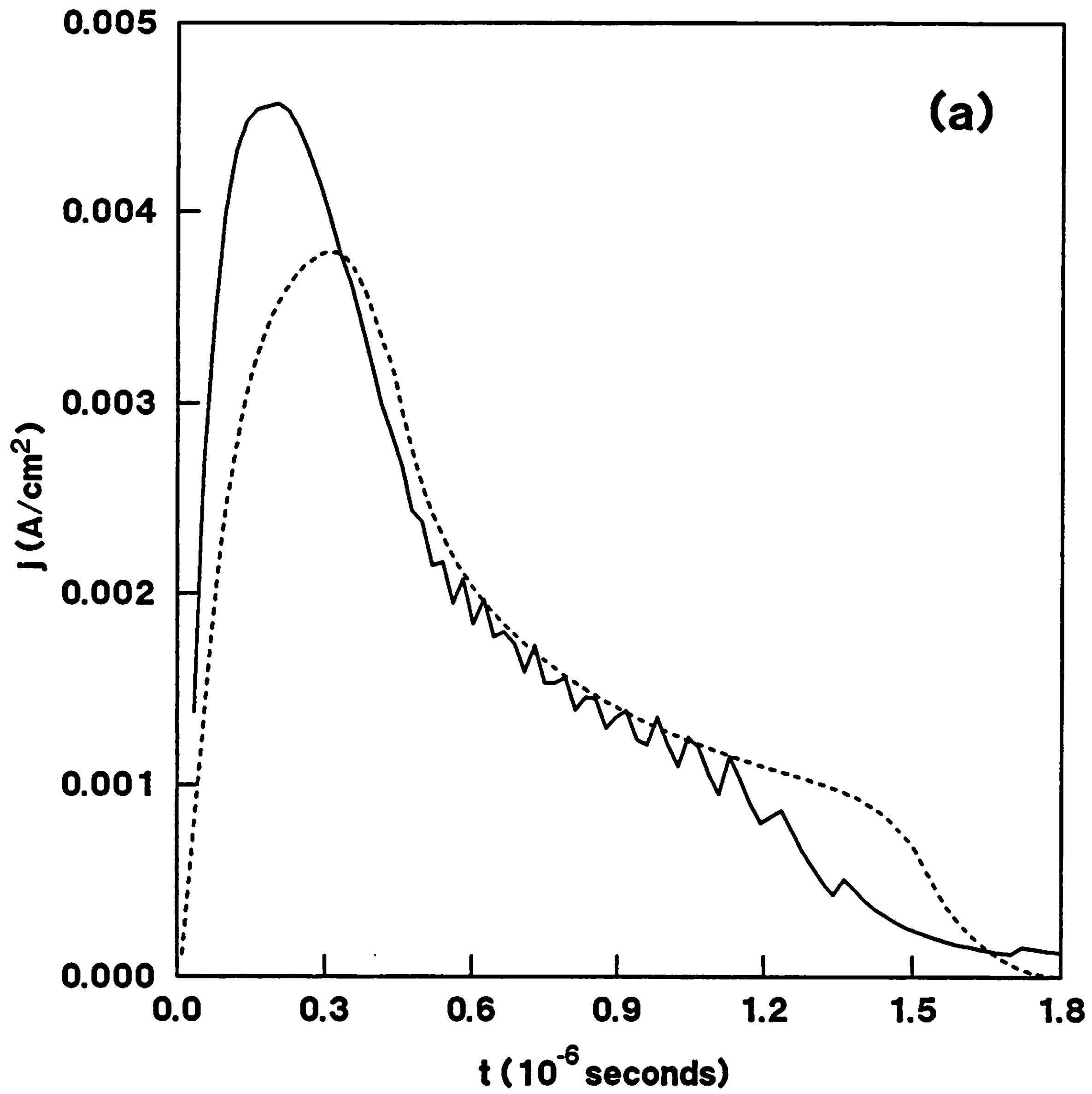

Figure 5(a)

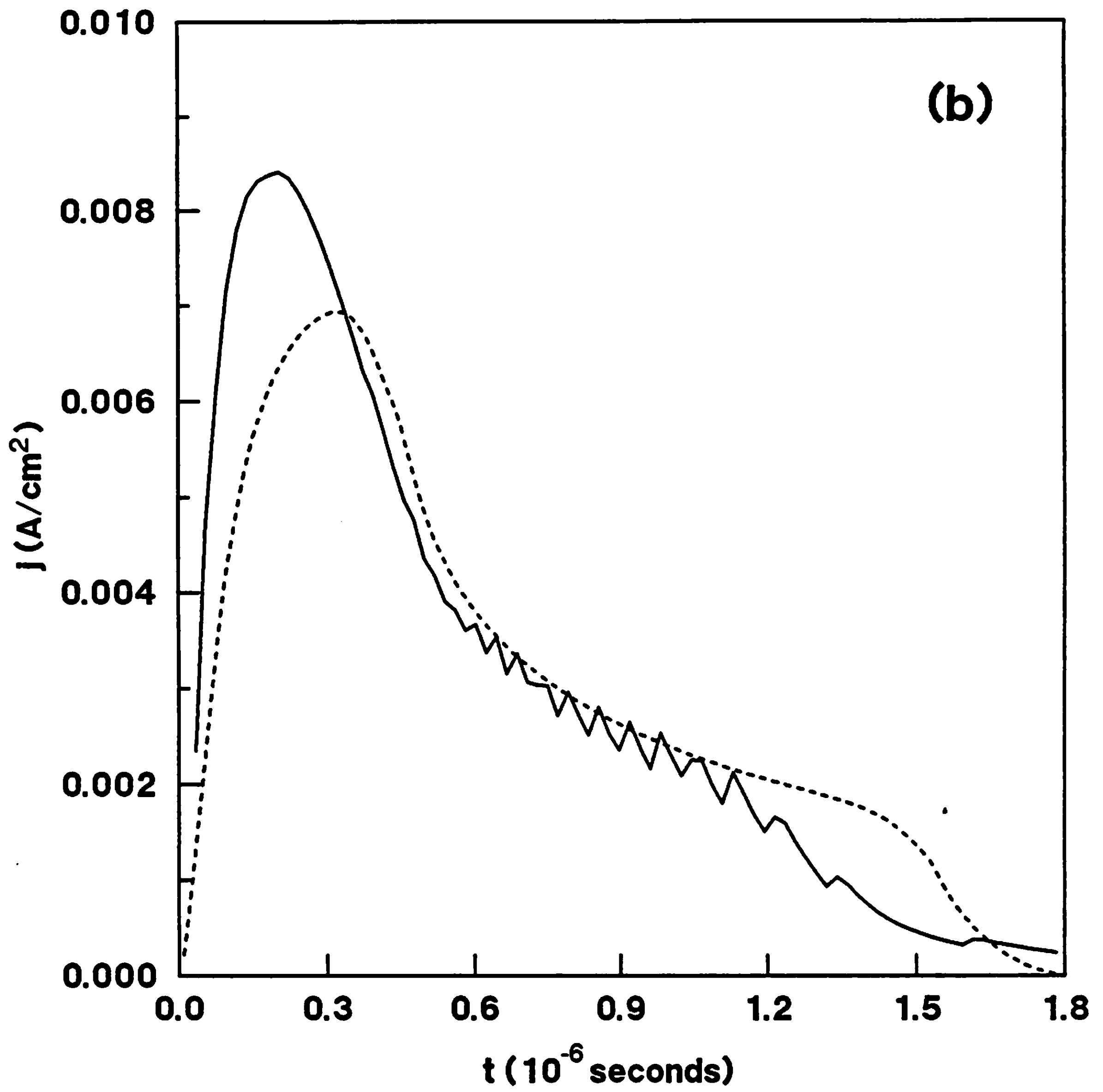

Figure 5(b)

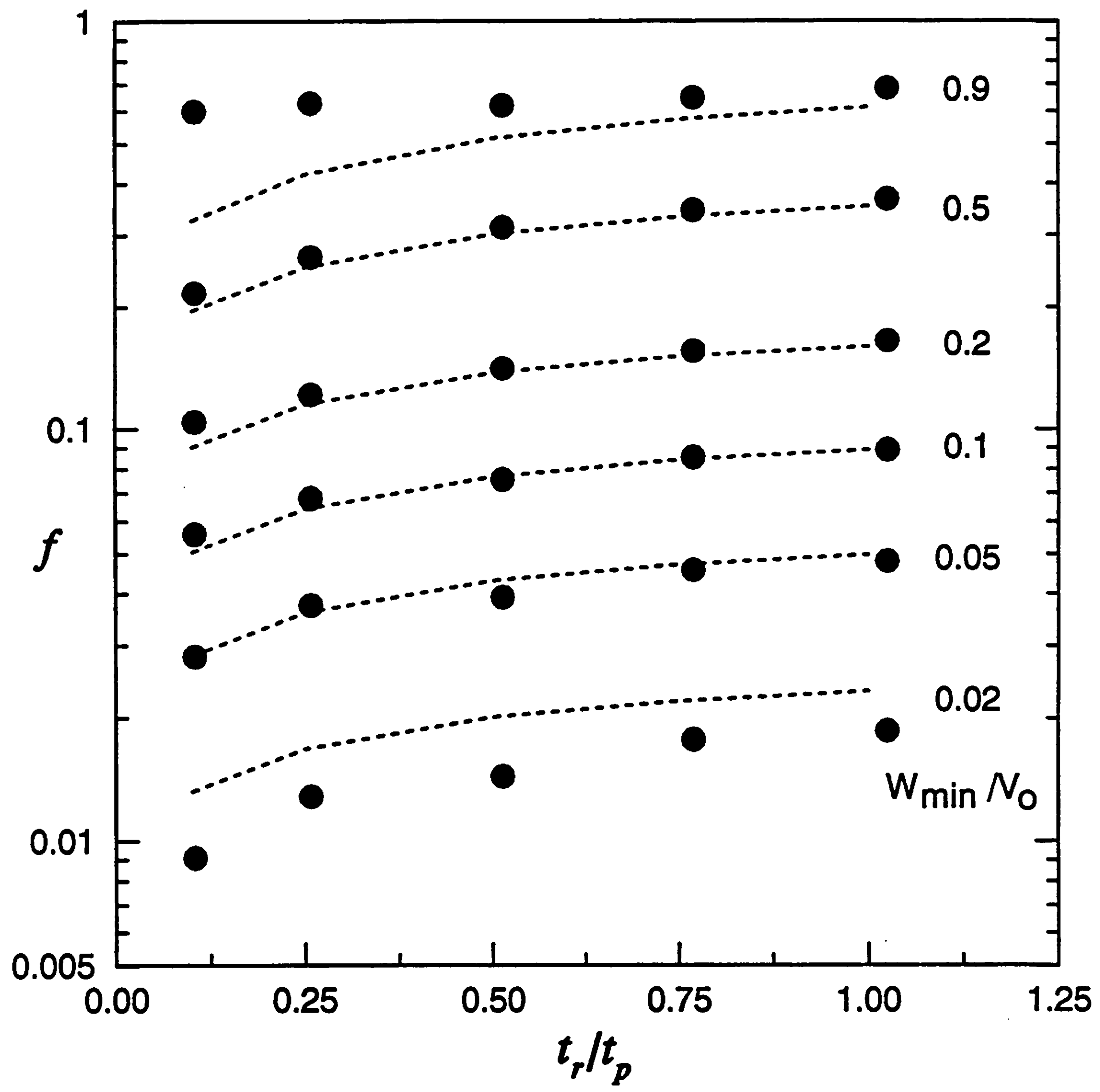

Figure 6